

Multiscale Mathematical Model with Discrete–Continuum Transition for Gas–Liquid–Slag Three-Phase Flow in Gas-Stirred Ladles

LINMIN LI^{1,4}, WENYANG DING,² FEIFEI XUE,¹ CHANG XU,¹
and BAOKUAN LI³

1.—College of Energy and Electrical Engineering, Hohai University, Nanjing 211100, China
2.—Institute of Thermal Science and Technology, Shandong University, Jinan 250061, China.
3.—School of Metallurgy, Northeastern University, Shenyang 110819, China. 4.—e-mail:
lilinmin@hhu.edu.cn

Gas–liquid–slag three-phase flow in a gas-stirred ladle is composed of both large-scale interfaces and discrete bubbles, making its modeling and study difficult. In the present work, a discrete–continuum transition model was incorporated into a hybrid Eulerian–Lagrangian model to comprehensively resolve the fluid flow in ladle metallurgy. The volume-of-fluid method was used to capture the large-scale interfaces, while a discrete bubble model was applied to simulate the small bubbles that cannot be resolved using the interface-capturing method. The transition between the small bubbles in Lagrangian coordinates and the large bubbles whose interfaces are captured is included using a newly developed algorithm to further reveal the bubble behaviors. Moreover, the complicated vortex structure is characterized using the large-eddy simulation approach. The present modeling framework enables the most complete analysis of gas–liquid–slag three-phase flow in ladles to date.

INTRODUCTION

Ar-gas stirring is widely employed in ladle furnaces to homogenize the chemical composition of alloy elements and the temperature field. In this method, the gas is divided into discrete bubbles after coming through a porous plug(s), which helps to remove inclusions and enhance the rates of refining reactions. The discrete bubbles can rise in haphazard fashion or may aggregate with each other, forming a turbulent bubble plume. When they pass through the slag layer, a complicated interface structure between slag and molten steel is also generated. Strong stirring is needed to promote efficient desulfurization and slag–steel intermixing, but formation of a large open eye is undesirable to avoid pick-up of O and N or entrainment of slag droplets. Moreover, calm flow with small bubbles is needed for inclusion removal. As a consequence, the bubble size can vary over a wide range and the features of the slag layer can be very complicated,

making it difficult to analyze the bubble behaviors and mixed flow phenomena in a gas-stirred ladle effectively.

The lack of combined modeling of discrete bubbles and continuous fluids is one of the most crucial shortcomings of current models of multiphase flows, although several mathematical models have been proposed to investigate the flow characteristics and slag-layer behaviors in gas-stirred ladles; For example, Li et al.¹ and Llanos et al.² adopted the volume-of-fluid (VOF) method to simulate the fluid dynamics of all phases in a ladle. Zhang,³ Luo and Zhu,⁴ and Li et al.⁵ used a multifluid model to simulate the flow of each phase. However, as these two methods cannot model the behaviors of individual bubbles dispersed in the liquid, a modeling framework that tracks discrete bubbles in Lagrangian coordinates while simulating the fluid flow in Eulerian coordinates was proposed by Guo et al.,⁶ Madan et al.,⁷ and Park and Yang,⁸ among others. Subsequently, to combine the benefits of the

Lagrangian discrete bubble model and interface tracking method, Liu et al.⁹ and Cloete et al.¹⁰ employed the discrete phase model (DPM) and the VOF method to simulate the bubble motion and interfacial behaviors of slag, respectively, applying the standard $k-\epsilon$ turbulence model. To better reveal the unsteady behaviors and interactions among different phases, Li et al.¹¹ used the large-eddy simulation (LES) approach along with the DPM–VOF model to simulate the unsteady phenomena in a water model of a ladle, and the modeling framework was continuously improved by considering bubble coalescence¹² and the transition between discrete bubbles and continuous gas.¹³ The resulting model for tracking the discrete bubbles was called the discrete bubble model (DBM).¹³ This combined modeling framework (LES–VOF–DBM) shows promise for modeling and effective analysis of gas–liquid–slag three-phase flow in a gas-stirred ladle by directly tracing the interfaces of the slag layer while calculating the motion of each bubble. The coupled behaviors of the gas bubbles, molten steel, and slag layer can be comprehensively studied, including bubble movement, bubble-size redistribution, slag-eye features, slag-droplet entrainment, etc. Despite all these achievements, problems still exist when using the above-mentioned approach, among which the most critical is that the discrete bubble model cannot simulate bubble deformation. Consequently, the model is not very suitable for modeling relatively large bubbles that are easily deformed. As seen from the experimental results in Fig. 1, bubbles are deformable especially when their diameter reaches approximately 5 mm. This experiment was conducted using a water model; the geometric parameters can be found in our previous work.⁵ The gas flow rate was 5 L/h, and the bath height was 700 mm.

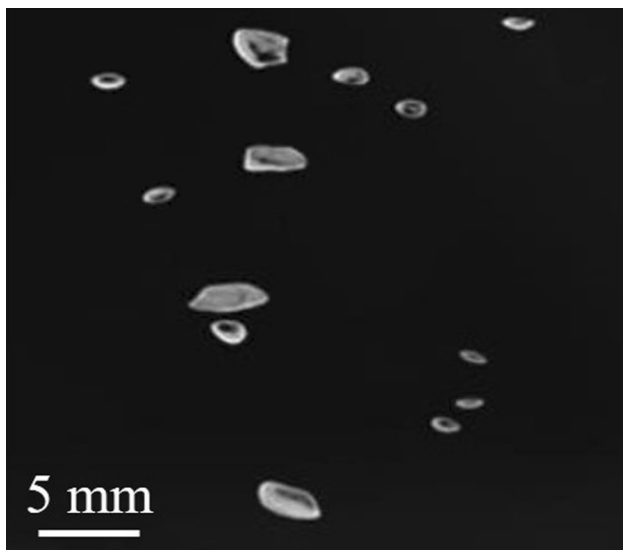


Fig. 1. Gas bubbles captured in a water model experiment.

The motivation for the present work is to provide a comprehensive model for gas–liquid–slag mixed flow in ladle metallurgy, for more effective study of the related phenomena and underlying mechanisms. As the aforementioned LES–VOF–DBM modeling framework only considers the transition between discrete bubbles and continuous gas at the top surface, we aim to incorporate a discrete–continuum transition model into the framework for gas bubbles and simulate the bubbles using a hybrid discrete–continuum method. Our concept is to capture the surface of large bubbles but track small bubbles using the DBM. In this way, the deformation of bubbles that are relatively large can be considered and multiphase flow features be revealed as completely as possible. Figure 2 shows diagrammatic sketches of the model proposed herein and the LES–VOF–DBM modeling framework from our previous work,¹³ to better illustrate the differences between them.

Model Formulation

In terms of the phase field, the present model is mainly composed of two aspects: the interface-capturing method in Eulerian coordinates (VOF) and the discrete bubble modeling approach in Lagrangian coordinates (DBM). As the solution precision of the interface-capturing method depends on the mesh resolution and the fact that bubbles smaller than the grid cannot be distinguished,¹⁴ the present work divides the bubbles into two types: subgrid-scale bubbles and large bubbles, which are solved using the DBM and VOF method, respectively. Additionally, the liquid–slag interface and the top surface are also directly resolved using the VOF method.

VOF Method

The VOF method models two or more immiscible fluids by tracking the interfaces among them. A detailed description of the VOF model can be found in the work of van Sint Annaland et al.¹⁵ Tracking of interfaces is accomplished by solution of a continuity equation for the volume fraction of one phase. For the k th phase, the continuity equation is expressed as

$$\frac{\partial \alpha_k}{\partial t} + \frac{\partial}{\partial x_i} (\alpha_k u_i) = 0. \quad (1)$$

In the present work, the volume-fraction equations for gas and slag are solved, while the volume fraction of liquid is constrained by $\alpha_{\text{liquid}} = 1 - \alpha_{\text{gas}} - \alpha_{\text{slag}}$. Besides, u represents the velocity, and the properties of the mixed fluid are calculated as

$$\rho = \alpha_{\text{liquid}} \rho_{\text{liquid}} + \alpha_{\text{gas}} \rho_{\text{gas}} + \alpha_{\text{slag}} \rho_{\text{slag}}, \quad (2)$$

$$\mu = \alpha_{\text{liquid}} \mu_{\text{liquid}} + \alpha_{\text{gas}} \mu_{\text{gas}} + \alpha_{\text{slag}} \mu_{\text{slag}}. \quad (3)$$

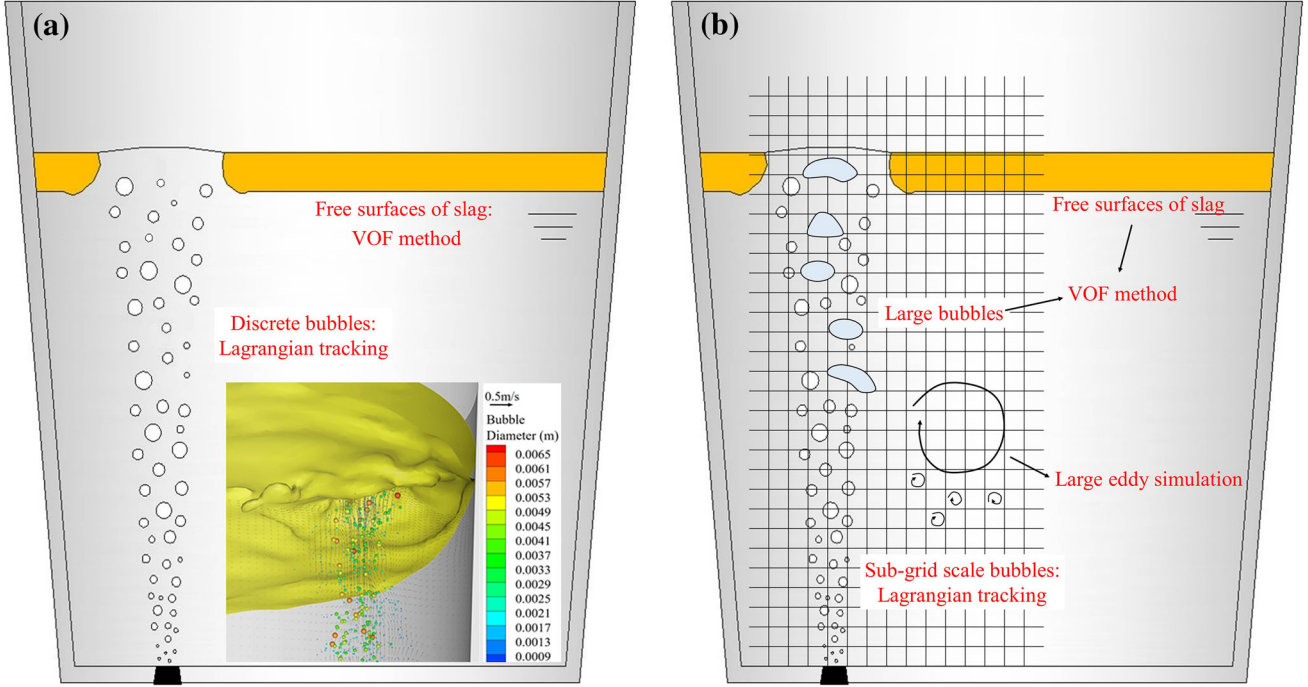


Fig. 2. Diagrammatic sketch of (a) LES-VOF-DBM modeling framework in previous work,¹³ and (b) current modeling framework.

LES Approach

In the VOF method, it is assumed that the velocity field is shared among the phases and a single set of momentum equations is solved throughout the domain. The governing equations employed for LES are obtained by filtering the time-dependent Navier–Stokes equations. The filtering process effectively filters out eddies that are smaller than the filter width or grid spacing used in the computations. The filtered Navier–Stokes equation can be written as

$$\frac{\partial(\rho\bar{u}_i)}{\partial t} + \frac{\partial(\rho\bar{u}_i\bar{u}_j)}{\partial x_j} = -\frac{\partial\bar{P}}{\partial x_i} + \frac{\partial}{\partial x_j} \left(\mu \left(\frac{\partial\bar{u}_i}{\partial x_j} + \frac{\partial\bar{u}_j}{\partial x_i} \right) \right) - \frac{\partial\tau_{ij}}{\partial x_j} + \rho g_i + F_s + F_b, \quad (4)$$

where P represents the pressure, g_i is the gravitational acceleration (if i represents the gravity direction), F_s and F_b are the surface tension and the resultant force caused by discrete bubbles, respectively, and τ_{ij} is the subgrid-scale (SGS) stress, defined by

$$\tau_{ij} = \rho(\bar{u}_i\bar{u}_j - \bar{u}_i\bar{u}_j). \quad (5)$$

The SGS stress resulting from the filtering operation is modeled using the following equations¹⁶:

$$\tau_{ij} - \frac{1}{3}\tau_{kk}\delta_{ij} = -2\mu_t\bar{S}_{ij}, \quad \bar{S}_{ij} = \frac{1}{2} \left(\frac{\partial\bar{u}_i}{\partial x_j} + \frac{\partial\bar{u}_j}{\partial x_i} \right), \quad (6)$$

where δ_{ij} is equal to 1 if $i = j$ and 0 otherwise, and μ_t is the SGS turbulent viscosity, calculated as

$$\mu_t = \rho \left(\min(\kappa d, C_S V^{1/3}) \right)^2 \sqrt{2\bar{S}_{ij}\bar{S}_{ij}}, \quad (7)$$

where κ is the von Kármán constant (set to 0.4), d is the distance to the closest wall, V is the volume of the cell, and C_S is the Smagorinsky constant, which is equal to 0.1.

The surface tension F_s in Eq. 4 is calculated using the continuum surface force (CSF) model¹⁷:

$$F_s = \sigma\gamma \frac{\partial\alpha}{\partial x_i}, \quad (8)$$

where σ is the surface tension coefficient and the curvature γ of the free surface is calculated as

$$\gamma = -\nabla \cdot (\nabla\alpha/|\nabla\alpha|). \quad (9)$$

The resultant force of discrete bubbles, F_b , acting on fluids is given in the next section.

Hybrid Discrete–Continuum Model of Bubbles

Discrete Bubble Model

The most important part of the present study is to implement a new model to simulate bubble behaviors by directly capturing the interfaces of large bubbles and tracking small discrete bubbles. The large bubbles are simulated as a continuum, and each small bubble is tracked individually in Lagrangian coordinates, thus constituting a hybrid discrete–continuum model. Basically, the motion of discrete bubbles is calculated using the following equation:

$$\frac{d\vec{u}_b}{dt} = \frac{\vec{g}(\rho_{\text{gas}} - \rho)}{\rho_{\text{gas}}} + \vec{F}_{\text{Drag}} + \vec{F}_{\text{VM}} + \vec{F}_{\text{PG}}, \quad (10)$$

where \vec{F}_{Drag} is the drag force, which is written as

$$\vec{F}_{\text{Drag}} = \frac{18\mu}{\rho_{\text{gas}} d_b^2} \frac{C_D Re}{24} (\vec{u} - \vec{u}_b), \quad (11)$$

where d_b is the bubble diameter and Re is the relative Reynolds number, defined as

$$Re = \frac{\rho d_b |\vec{u}_b - \vec{u}|}{\mu}. \quad (12)$$

Although small bubbles are less deformable, a drag coefficient law more suitable for bubbles proposed by Ishii and Zuber¹⁸ is used for the drag coefficient C_D . The additional acceleration terms are the virtual-mass force \vec{F}_{VM} and pressure-gradient force \vec{F}_{PG} , which are expressed as

$$\vec{F}_{\text{VM}} = C_{\text{VM}} \frac{\rho}{\rho_{\text{gas}}} \left(\vec{u}_b \nabla \vec{u} - \frac{d\vec{u}_b}{dt} \right), \quad (13)$$

$$\vec{F}_{\text{PG}} = \frac{\rho}{\rho_{\text{gas}}} \vec{u}_b \nabla \vec{u}, \quad (14)$$

where C_{VM} is the virtual-mass force coefficient, equal to 0.5. These two forces are significant in bubble–liquid systems and are thus considered in the present work. The interaction between bubbles and liquid, F_b , is the resultant force of drag, the virtual-mass force, and the pressure-gradient force, and the change in momentum of both bubbles and fluids is evaluated as bubbles pass through each control volume to achieve the two-way coupling.

Discrete–Continuum Transition

In the present work, the large bubbles that can be distinguished by the mesh are solved as continua by tracking their surfaces using the VOF method. Owing to the aggregation and growth of bubbles, some discrete bubbles should change to continua. The model for bubble aggregation is omitted here and can be found in our previous work.¹³ To consider the discrete–continuum transition, the continuity equation of the gas volume fraction is written as

$$\frac{\partial \alpha_{\text{gas}}}{\partial t} + \frac{\partial}{\partial x_i} (\alpha_{\text{gas}} u_i) = S_b, \quad (15)$$

where S_b represents the source due to the transition between discrete bubbles and continuous gas. It contains two parts: one is the transition at the gas–liquid interface when a discrete bubble attaches to the continuous gas; the other is the transition when a discrete bubble grows to a large bubble that can be solved using the continuous method. Diagrammatic sketches of these two kinds of transition are shown in Fig. 3.

For the first kind of transition, when the bubble attaches to the gas–liquid interface ($\alpha_{\text{gas}} = 0.5$), we

stop tracking it and remove it from the system. Once a bubble is removed, the data for the volume fraction and velocity in the current cell are updated using the following equations:

$$\alpha_{\text{gas}} = \alpha_{\text{gas}} + V_b/V_{\text{cell}}, \quad (16)$$

$$\vec{u} = \vec{u} + V_b \vec{u}_b/V_{\text{cell}}, \quad (17)$$

where V represents the volume.

For the second type of transition, we also remove the bubbles whose volume is larger than the cell volume, and the source term in Eq. 15 is written as

$$S_b = V_b/(V_{\text{cell}} \cdot \Delta t). \quad (18)$$

Note that the above equation is only run once after the bubble is removed. Finally, the discrete–continuum transition is achieved so that the behaviors of both small and large bubbles can be comprehensively studied.

Numerical Details

Simulations were performed for the water-model experiment, the details of which can be found in our previous works.^{5,13} Water and soya bean oil were used to simulate the molten steel and slag layer, respectively. N_2 is used as the stirring gas, injected through a nozzle made of porous mullite to make it dispersed. The outlet of the nozzle is set as the inlet of discrete bubbles, whose size and number are specified, and the top of the ladle is set as the pressure outlet, which is specified as standard atmospheric pressure, while other boundaries are set as no-slip walls. Details of the geometric parameters and material properties are presented in Table I.

The domain is divided into hexahedral elements, whose size is determined as follows: the grid size at the inlet where bubbles are injected is approximately 4 mm, the maximum grid height is approximately 8 mm, and in the region where slag is present, the grid height is narrowed to 4 mm. Thus, bubbles with diameter above 6 mm (for an equivalent volume) can be directly resolved by the interface-capturing method. The total number of cells is approximately 500,000, and the time step Δt is set to 1×10^{-4} s. For pressure–velocity coupling, the pressure-implicit with splitting of operators (PISO) algorithm is used. To ensure that the gas flow rate is identical to that used in the experiment, the number of bubbles injected per unit time at the inlet is calculated as

$$N_{\text{in}} = \frac{6Q}{\pi d_{\text{bi}}^3}, \quad (19)$$

where Q is the gas flow rate and d_{bi} is the initial bubble diameter. According to experimental observations, the diameter of bubbles emerging from the plug is about 1 mm. Thus, the initial bubble diameter was set to 1 mm in the present work.

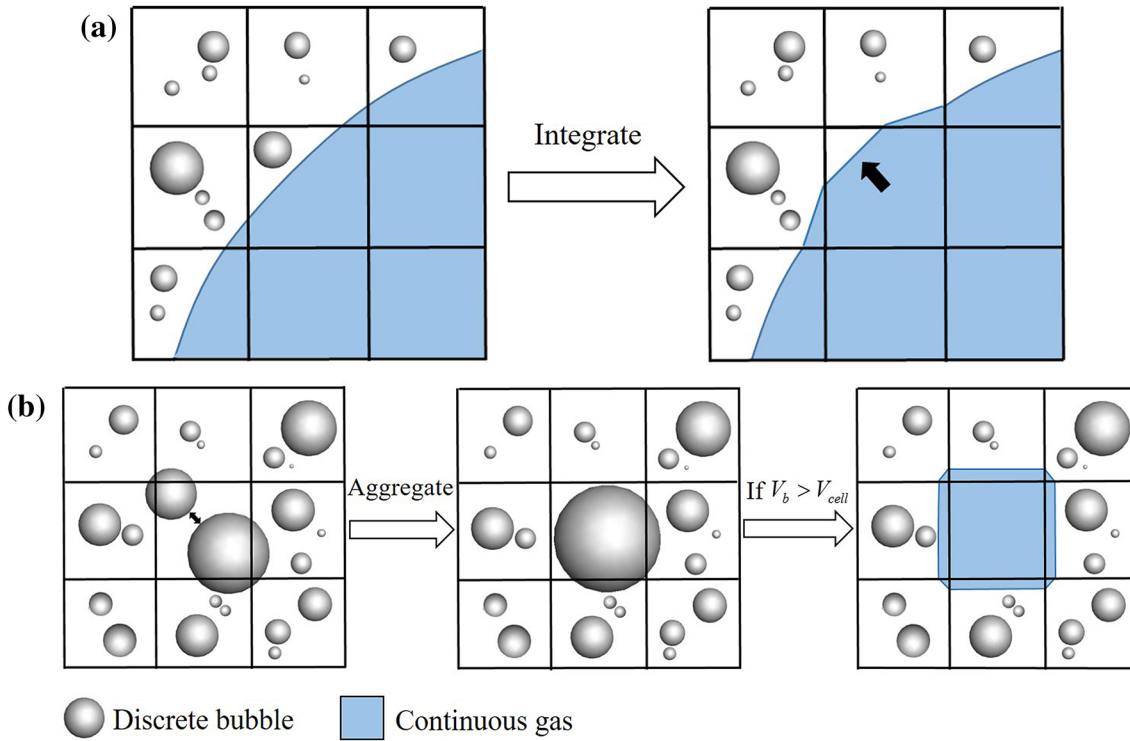


Fig. 3. (a) Integration between discrete bubbles and continuous gas, and (b) transition from discrete bubbles to continuous gas.

Table I. Simulation parameters

Geometric parameter	Value
Bottom diameter (mm)	617
Slope angle ($^{\circ}$)	2.44
Water depth (mm)	700
Slag layer thickness (mm)	40
Porous plug diameter (mm)	43.4
Plug radial position	0.67R
Material property	Value
Water density (kg m^{-3})	1000
Water viscosity ($\text{kg m}^{-1} \text{s}^{-1}$)	0.001
Oil density (kg m^{-3})	900
Oil viscosity ($\text{kg m}^{-1} \text{s}^{-1}$)	0.058
Gas density (kg m^{-3})	1.138
Gas viscosity ($\text{kg m}^{-1} \text{s}^{-1}$)	1.663×10^{-5}

RESULTS AND DISCUSSION

Bubble Behaviors

Discrete Bubble Aggregation

Simulations were performed for different gas flow rates of 90 L/h, 110 L/h, 130 L/h, and 150 L/h. The conditions were confirmed by setting up different bubble injection parameters. First, after bubbles were injected into the system, aggregation of discrete bubbles happens frequently in the lower part of the ladle. The present model simulates the small bubbles in Lagrangian coordinates, and each bubble

is individually tracked by modeling the aggregation among them. The discrete bubble distribution in the lower part of the ladle, the aggregation between two bubbles in the simulation ($Q = 90$ L/h), and comparison of the bubble diameter evolution between experiment and simulation are shown in Fig. 4.

It is found that the present model effectively shows the discrete bubble movement as well as the corresponding behaviors, enabling comprehensive simulation of the bubbles whose surface cannot be distinguished. The evolution of the time-averaged bubble diameter versus height showed good agreement with experimental data. Moreover, the result of the discrete bubble model is also more comprehensive than the multifluid model, which can only provide volume-averaged results for discrete bubbles. More detailed results regarding the bubble behaviors and bubble-size distributions can be found in our previous work.¹³

Discrete–Continuum Coupled Behaviors

For conditions with relatively high gas flow rates, some bubbles may become large enough to be simulated using the interface-capturing method. Using the algorithm for the discrete–continuum transition, the above-mentioned two types of transition can be modeled. Moreover, as some bubbles are solved using the discrete method and some are solved as continua, coalescence between large bubbles whose interfaces are captured can be directly resolved, while coalescence between large bubbles and discrete bubbles is modeled using the

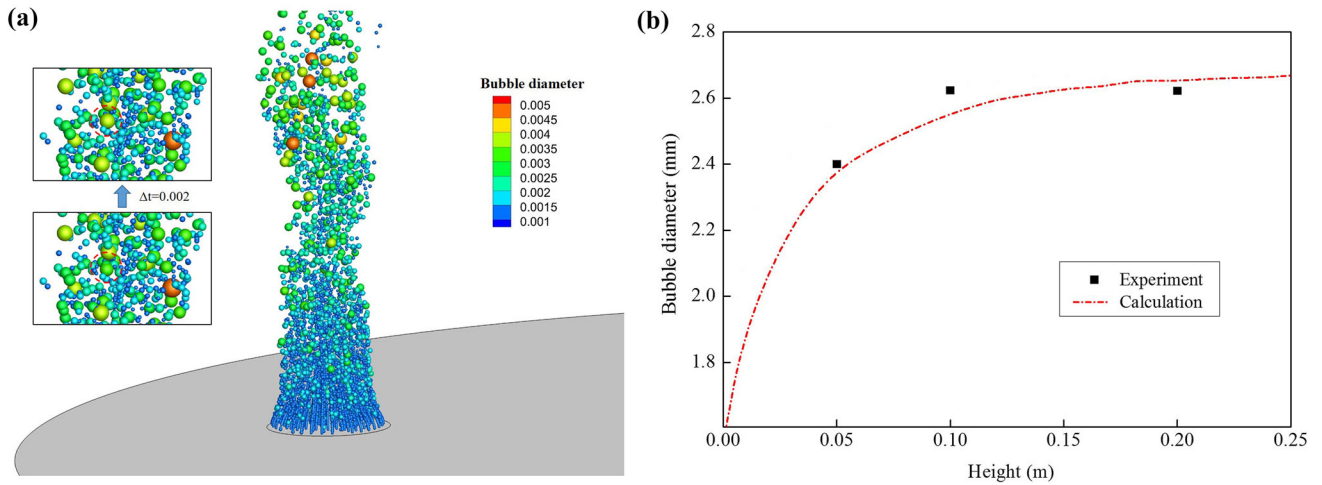


Fig. 4. (a) Bubble distribution above the inlet and discrete bubble aggregation process in the simulation ($Q = 90$ L/h), and (b) comparison of bubble diameter evolution between experiment and simulation.

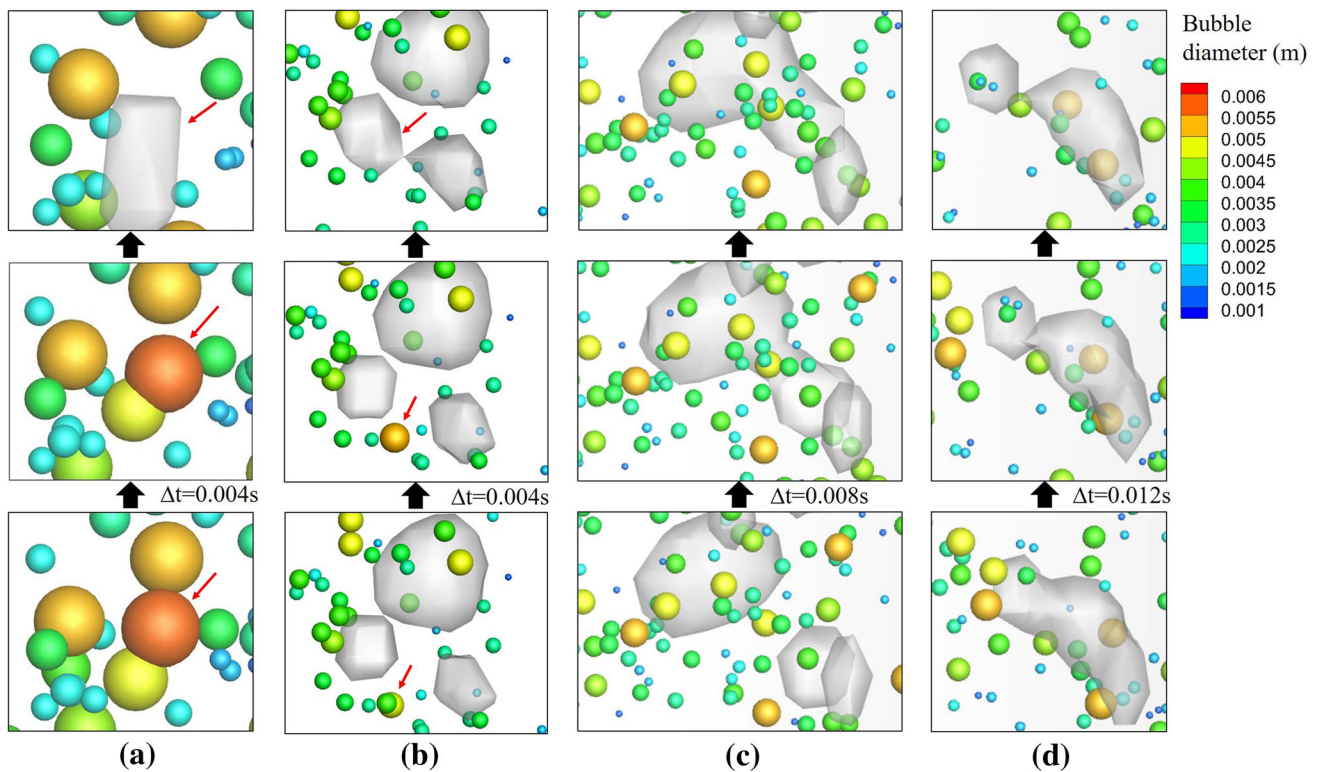


Fig. 5. Simulation results for discrete–continuum coupled behaviors of bubbles: (a) discrete–continuum transition, (b) discrete–continuum coalescence, and large bubble (c) coalescence and (d) breakage.

discrete–continuum transition model. Transient simulation results for the discrete–continuum transition, discrete–continuum coalescence, and large bubble coalescence and breakage are all shown in Fig. 5.

Each subfigure shows three instants for the corresponding behavior. Figure 5a shows two discrete bubbles moving toward each other and aggregating. Because the resulting bubble is large enough to be captured by the mesh, it is changed to be

solved as a continuum using the VOF method and its interface is tracked thereafter. Second, as large bubbles are generated and move upward with discrete bubbles, coalescence between discrete bubbles and large bubbles will occur. In Fig. 5b, two small bubbles aggregate into a larger one at the second instant, then when it touches the interface of the large bubble, discrete–continuum coalescence between them occurs. Consequently, the discrete bubble is removed and the large bubble size

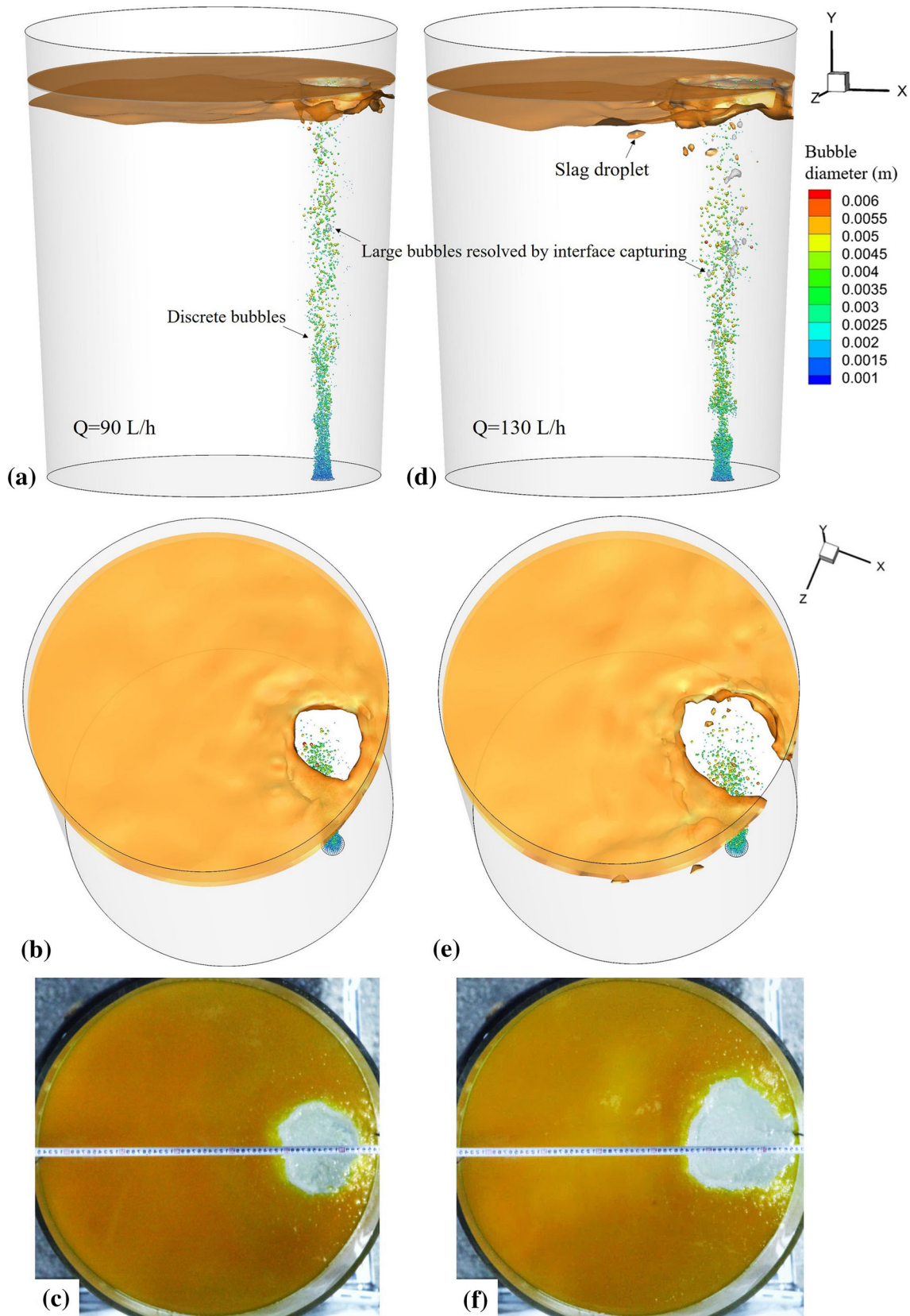


Fig. 6. Simulation results and experimental observations of slag-layer features with different gas flow rates: (a–c) 90 L/h and (d–f) 130 L/h.

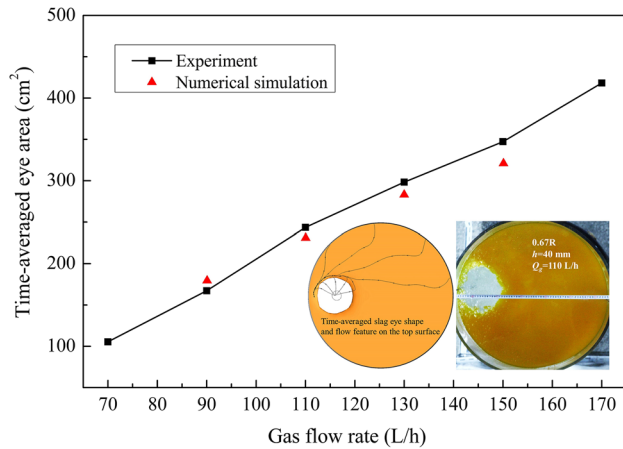


Fig. 7. Comparison of slag-eye size between experiment and simulations.

increases by receiving the mass of the discrete bubble.

As the interfaces of large bubbles are tracked, their coalescence and breakage can be resolved directly, as demonstrated in Fig. 5c and d. Moreover, it can be found that the maximum diameter of discrete bubbles in the field is approximately 6 mm, as larger ones are resolved by capturing and tracking their interfaces. It can be concluded that the bubble behaviors can be comprehensively revealed by dividing the bubbles into large and small ones and solving them within the newly developed modeling framework for simulation of bubbles. The hybrid discrete–continuum model with their coupling overcomes the shortcomings that the discrete method cannot consider deformation of large bubbles while the continuum method cannot resolve subgrid-scale bubbles.

Slag-Layer Behaviors

Unsteady Features

The behavior of the slag layer is another crucial aspect in ladle metallurgy, namely that mixing in the spout-eye area promotes efficient desulfurization, but also causes problems such as pick-up of O and N and entrainment of slag droplets. In the present work, we adopted the VOF method to simulate and investigate the interfacial flow of the slag layer. The results for the features of the slag layer and the gas-bubble distributions for different gas flow rates are shown in Fig. 6. The interfaces among gas, slag, and liquid are displayed using isosurfaces, while the discrete bubbles are plotted as spheres having the real size of bubbles. Figure 6a and b show simulation results from the side and top view, respectively, while Fig. 6c shows the experimental observation of the slag layer, for gas flow rate of 90 L/h. On the other hand, Fig. 6d, e, and f shows corresponding results for a higher gas flow rate of 130 L/h.

It is found that, with the higher gas flow rate, more large bubbles and slag droplets are generated. The spout-eye size also becomes larger. The predicted slag-layer features and eye size show qualitative agreement with the experimental observations. These results confirm that the present modeling framework can effectively reveal slag-layer behaviors including interface fluctuation, slag-droplet entrainment, spout-eye formation, etc.

Time-Averaged Slag-Eye Size

For quantitative validation, time-averaged results were evaluated from the transient simulations. Figure 7 shows the time-averaged slag-eye size obtained from both experiment and simulation, with an example of the time-averaged slag-eye features from the simulation and an instant from the experiment when the slag-eye size was close to the time-averaged value. The streamlines show that the gas–liquid mixture takes the slag to the periphery and then goes downward, while the slag on the top goes to the spout eye then also goes downward at the edge of the eye to form a loop. The results are in good agreement, indicating that the present model can predict the slag-eye size accurately.

CONCLUSION

A new multiscale modeling framework that directly tracks large-scale interfaces and models small discrete bubbles is proposed for gas–liquid–slag three-phase flow in a ladle. Most importantly, as the bubble size varies over a wide range, especially for high gas flow rates, and directly resolving all the bubble surfaces would require a large amount of computational resources, the gas bubbles are divided into large ones and small ones for multiscale simulation. The large bubbles are treated as continua and directly resolved by capturing the interfaces, while the small bubbles are modeled using the discrete bubble model by considering bubble aggregation. The coupling between small and large bubbles or continuous gas is achieved using a discrete–continuum transition algorithm developed in this work. Bubble behaviors including aggregation and breakage can be completely resolved within a certain mesh resolution. Moreover, slag-layer behaviors are also well revealed, and the slag-eye size agrees well with experimental data. The present work represents only a preliminary investigation into the developed model. More detailed study will be presented in our future work.

ACKNOWLEDGEMENTS

The authors are grateful for support from the Fundamental Research Funds for the Central Universities (Grant No. 2018B01614) and the China Postdoctoral Science Foundation (Grant No. 2018M630502).

REFERENCES

1. B. Li, H. Yin, C. Zhou, and F. Tsukihashi, *ISIJ Int.* 48, 1704 (2008).
2. C.A. Llanos, S. Garcia, J.A. Ramos-Banderas, J.D.J. Barreto, and G. Solorio, *ISIJ Int.* 50, 396 (2010).
3. L. Zhang, *Modell. Simul. Mater. Sci. Eng.* 8, 463 (2000).
4. W. Lou and M. Zhu, *Metall. Mater. Trans. B* 44, 1251 (2013).
5. L. Li, Z. Liu, B. Li, H. Matsuura, and F. Tsukihashi, *ISIJ Int.* 55, 1337 (2015).
6. D.C. Guo, L. Gu, and G.A. Irons, *Appl. Math. Model.* 26, 1457 (2002).
7. M. Madan, D. Satish, and D. Mazumdar, *ISIJ Int.* 45, 677 (2005).
8. H.J. Park and W.J. Yang, *Numer. Heat Transf. A* 31, 493 (1997).
9. H. Liu, Z. Qi, and M. Xu, *Steel Res. Int.* 82, 440 (2011).
10. S.W.P. Cloete, J.J. Eksteen, and S.M. Bradshaw, *Miner. Eng.* 46–47, 16 (2013).
11. L. Li, Z. Liu, M. Cao, and B. Li, *JOM* 67, 1459 (2015).
12. L. Li and B. Li, *JOM* 68, 2160 (2016).
13. L. Li, B. Li, and Z. Liu, *ISIJ Int.* 57, 1980 (2017).
14. L. Li and B. Li, *Particuology* 39, 109 (2018).
15. M. van Sint Annaland, N.G. Deen, and J.A.M. Kuipers, *Chem. Eng. Sci.* 60, 2999 (2005).
16. J. Smagorinsky, *Mon. Weather. Rev.* 91, 99 (1963).
17. J.U. Brackbill, D.B. Kothe, and C. Zemach, *J. Comput. Phys.* 100, 335 (1992).
18. M. Ishii and N. Zuber, *AIChE J.* 25, 843 (1979).